ARTICLE

Quantitative Measurement of Cation-Mediated Adhesion of DNA to Anionic Surfaces

Received 00th January 20xx, Accepted 00th January 20xx

DOI: 10.1039/x0xx00000x

Xian Hao, +ab Qufei Gu, +c Christine Isborn, Makenzie Provorse Long, *d Jesus Rodriguez Vasquez, and Tao Ye*ac

Anionic polyelectrolytes, such as DNA, are attracted to anionic surfaces in the presence of multivalent cations. A major barrier toward molecular-level understanding of these attractive interactions is the paucity of measurements of the binding strength. Here, atomic force microscopy-based single molecule force spectroscopy was used to quantify the binding free energy of double-stranded DNA to an anionic surface, with complementary density functional theory calculations of the binding energies of metal ion-ligand complexes. The results support both electrostatic attraction and ion-specific binding. Our study suggests that the correlated interactions between counterions are responsible for attraction between DNA and an anionic surface, but the strength of this attraction is modulated by the identity of the metal ion. We propose a mechanism in which the strength of metal-ligand binding, as well as the preference for particular binding sites, influence both the concentration dependence and the strength of the DNA-surface interactions.

Introduction

Anionic polyelectrolytes, such as DNA, RNA, anionic polysaccharides, and certain proteins, 1, 2 are attracted to anionic 3, 4 or zwitterionic surfaces in the presence of multivalent cations. The attraction underlies a variety of applications, such as confining these polyelectrolytes (DNAs, RNAs, and proteins) to solid-liquid interfaces for self-assembly into 2D hierarchical structures, 4-6, 7 surface immobilization of biomolecules for high resolution atomic force microscopy (AFM) imaging, 3, 8-10 purification of nucleic acids, formation of nucleic acid-liposome complexes for vaccine development, and gene therapy. 11 Multivalent cations also mediate attraction between anionic macromolecules or assemblies, which drive a range of aggregation and assembly phenomena in biology, including formation of microtubules, 12 condensation of DNA, 13, 14 aggregation of amyloid proteins, 15, 16 and membrane fusion. 17

Much remains unknown concerning the molecular level origin of the cation-mediated attraction. Mean-field Poisson Boltzmann theory commonly used to treat electrostatic interactions predicts net repulsion between two like-charged surfaces, regardless of the valence of the counterions. Numerous theoretical studies rationalized such attractive interactions by considering the discrete nature of the counterions and invoking correlated binding. In this mechanism, each of the anionic surfaces is in contact with a mobile layer of multivalent cations (counterions). In these surfaces

are in close proximity, the binding of counterions within the two mobile layers becomes strongly correlated, leading to staggered cation configurations that minimize the overall energy and produce a net attractive interaction (Scheme 1A). 19-21 Although Monte Carlo and hypernetted chain theory simulations depicting such counterion correlation have qualitatively reproduced these effective attractive interactions, 19, 21, 23, 24 this electrostatic model predicts similar interaction strengths for cations with the same valence. However, experimental studies indicate that the attraction strength may differ for different divalent cations. 6, 25, 26 Such ion specificity could be more readily rationalized by multivalent cations directly bridging the two anionic surfaces through metal-ligand interactions (Scheme 1B).3,5 This ion-bridging mechanism may explain the stronger adsorption of DNA to mica surfaces induced by divalent transition metal ions compared to Mg²⁺.^{3, 5} Overall, it is not clear the extent to which ion correlation and ion bridging mechanisms contribute to multivalent cation-mediated attraction of anionic surfaces.

A major barrier toward molecular level understanding of the multivalent cation-mediated attraction is the paucity of quantitative measurement of the interaction strength. For example, in studies of DNA-surface interactions, the strength of these interactions was inferred from the surface coverage of adsorbed DNA.³ Other studies inferred the strength of the interactions from either the mobility or clarity of features in the AFM images.^{6, 25, 26} Although these measurements yielded some qualitative trends, quantitative information concerning the interaction strength could not be derived from these observables. Therefore, the measurement of the binding free energy, arguably the most direct experimental observable, is needed to further our understanding of the multivalent cation-mediated attraction between anionic surfaces in order to precisely control such interactions for technological applications.

Here we present a systematic study of the binding free energy of a double-stranded DNA (dsDNA), a model anionic polyelectrolyte, to

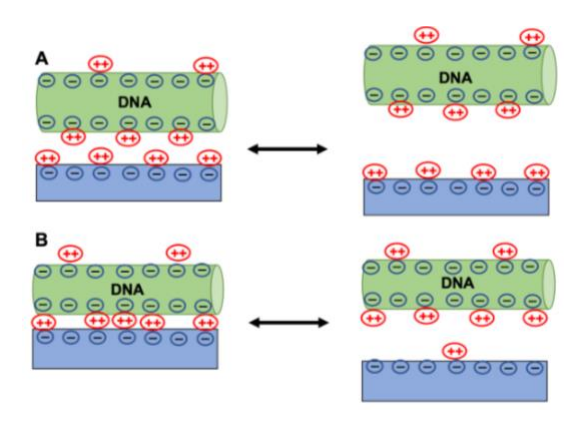
^a Department of Chemistry and Biochemistry, School of Natural Sciences, University of California, Merced, California, 95343, United States.

b. School of Public Health and Jiangxi Provincial Key Laboratory of Preventive Medicine, Nanchang University, Nanchang, Jiangxi, 330006, China.

C. Materials and Biomaterials Science and Engineering, School of Engineering, University of California, Merced, California, 95343, United States.

^{d.} Department of Chemistry and Biochemistry, Creighton University, Omaha, Nebraska, 68178, United States.

[†] These authors contribute equally to the work.



Scheme 1. Mechanisms for cation-mediated adhesion of DNA to an anionic surface. (A) Strong correlation between cations in the two mobile condensed layers leads to net positive charges and negative charges, maximizing attractive interactions between the two surfaces. (B) Attraction is caused by multivalent cations bridging the adsorption sites through metal-ligand interactions.

an anionic self-assembled monolayer (SAM) surface in the presence of Ni²⁺, Co²⁺, and Mg²⁺ divalent cations. Using AFM-based single molecule force spectroscopy^{27, 28} that repeatedly adsorbs and desorbs tip-tethered DNA molecules on a highly ordered SAM that is terminated with carboxylate groups (Figure 1A) under quasi-equilibrium conditions, we measured the desorption forces and calculated the binding free energy per base pair under different buffer compositions. These experimental measurements are complemented by density functional theory calculations of the binding energies of metal ion-ligand complexes.

Experimental and computational methods

Preparation of Self-Assembled Monolayer Surface

A monolayer of 11-mercaptoundecanoic acid (MUDA, Sigma Aldrich, St. Lois, MO, USA) was prepared by overnight immersion of a clean Au (111) substrate into a 1 mM solution of the thiol in 9:1 (v/v) ethanol:acetic acid. After immersion, the Au substrate was rinsed with 9:1 (v/v) ethanol:acetic acid and then deionized water.

Functionalization of AFM Tip with Long DNA

A dsDNA, ~1 kbp or 340 nm in length, was attached to the AFM tip using a method reported previously. ²⁹ The contour length is significantly larger than the persistence length of dsDNA, 50 nm. Briefly, Au-coated Si₃N₄ AFM tips (Model NPG-10, Bruker, Santa Barbara, CA, USA) with a nominal spring constant of ~0.06-0.12 N/m was functionalized with a monolayer of 11-mercaptoundecanoic acid. Thiolated anchor DNA strands were attached by "inserting" into the monolayer. ³⁰, ³¹ These anchor strands can hybridize then crosslink with the single stranded tail on double-stranded DNA. More details can be found in the electronic supporting information (ESI).

Single Molecule Force Measurements

Single-molecule force spectroscopy analysis was performed using a Keysight 5500 AFM (Keysight Technologies, Santa Rosa, CA, USA) operating under contact mode in a 0.1 \times TAE (Tris(hydroxymethyl)aminomethane acetate and EDTA) buffer

containing varying concentrations of divalent cations. An approach/retract velocity of 400–500 nm/s and a typical loading rate of the applied force on the cantilever ranging from 300 to 500 pN/s was used to measure DNA-surface interactions. A total number of 2000-3000 approach/retraction curves were collected in each experiment, depending on the DNA-immobilized AFM tip, the approach/retraction velocity, the applied loading rate, the DNA conjugation chemistry and the SAM surface. The adhesion force (F) between the DNA and the surface is proportional to the cantilever deflection through Hooke's law:

$$F = k \times s \times v \tag{1}$$

where k is the spring constant (in pN/nm), s is the deflection sensitivity (in nm/volt), which allows conversion from the photodiode deflection signal to the deflection distance, and v is the deflection (in volts). The spring constant (k) was calibrated by the thermal noise fluctuation method³² using LabView (National Instruments, Austin, TX, USA):

$$k = 0.778 \frac{k_B T}{(\Delta h)^2} \tag{2}$$

where k_B is the Boltzmann constant, T is the temperature, and Δh is the cantilever deflection. The deflection sensitivity (s) was determined by the inverse slope of the linear portion of the force/distance curve (nm/volt), where the tip was in direct contact with the surface. To determine the DNA/surface adhesion force, a built-in MATLAB (MATLAB Inc., Waltham, MA, USA) function named edge detection was utilized to identify the boundaries of the force plateau in force/distance curves. The average plateau height between the two plateau edges, which represents the cantilever deflection, was then converted to mean adhesion forces using (1). The plateau distance, which corresponds to the length of the portion of the tethered DNA that is interacting with the opposing monolayer surface, was determined as the distance between the two edges of the plateaus. An ideal plateau distance of ~335 nm, corresponding to the full contour length of 1031 bp target DNA, was rarely observed in our measurements. Previous studies have shown that the contour length and the persistence length of DNA immobilized onto an anionic surface by divalent cations are close to what is expected for B-DNA in solution.^{3, 29, 33, 34} Moreover, existing non-contact AFM studies of dsDNA immobilized by Ni2+ onto anionic surfaces35, 36 showed that the secondary structure of the adsorbed DNA is similar to the native structure in the solution, suggesting that dsDNA is not significantly deformed by adsorption. In general, the recorded force plateaus were less than 300 nm in length depending on the tip geometry, the applied loading rate, and the DNA conjugation chemistry. To exclude cases involving nonspecific tip-sample interactions, force/distance curves with plateau distance < 20 nm were not included in the analysis.

Computational Methods

Density functional theory (DFT) calculations of small-molecules and clusters provide physical insight about the local metal-ligand interactions that contribute to more complex phenomena, including metal ion binding to carboxylate-terminated monolayers.³⁷⁻³⁹ Minimum-energy structures modeled by DFT have been used to rationalize ion selectivity by predicting relative metal-ligand binding

strengths and preferred binding motifs. 40-43 These local metal-ligand interactions can be used to analyze and deepen understanding of more complex interactions. As examples, minimum-energy structures of a Ca²⁺-acetate complex reproduce experimental vibrational frequencies of a carboxylate-terminated self-assembled monolayer measured in CaCl₂ solution,⁴⁴ optimized structures of Mg²⁺ carboxylate complexes give insight to binding in metalloproteins,45 and small structural models are often used to model ion coordination in enzymes, such as comparing the binding of ligands to Mg²⁺ and Mn²⁺ to interpret the binding preference in glycosyltransferases.46 In this work, DFT was used to compute the direct and indirect binding energies of Ni²⁺, Co²⁺, and Mg²⁺ with phosphate and guanine (model molecules for DNA binding) as well as carboxylate, a model for the SAM surface ligand. Indirect binding (i.e., outer-sphere or solvent-shared ion pair) is mediated by hydrogen bonds between water molecules in the ion's first solvation shell and the binding site. Direct binding (i.e., inner-sphere or contact ion pair) occurs when a hydrated metal ion loses at least one water molecule from its first solvation shell and forms a direct contact with the binding site. The small-molecule complexes were used to model local metal-ligand interactions for the possible binding sites and motifs reported in the literature for both DNA⁴⁷⁻⁵⁴ and carboxylateterminated monolayers.^{38, 55} Mg²⁺ ions bind directly or indirectly at the DNA phosphate backbone and the N7 or O6 atoms of the guanine residue in the major groove of DNA.⁴⁷⁻⁵⁴ Ni²⁺ and Co²⁺ ions prefer to bind directly to the N7 atom of guanine but also bind to the phosphate backbone of DNA.^{48, 52, 53} Mg²⁺ and Ni²⁺ ions bind directly or indirectly to anionic carboxylate-terminated monolayers.^{38, 55} For direct binding, all three ions (Mg²⁺, Ni²⁺, and Co²⁺) prefer to bind to one atom (i.e., monodentate) instead of two atoms (i.e., bidentate) at the binding site. 38, 52, 53, 55 Minimum-energy structures of each metal-complex were surrounded by a polarizable dielectric continuum to account for long-range electrostatic effects. The binding energy for indirect binding ($BE_{indirect}$) was calculated as:

$$BE_{\text{indirect}} = E[M^{2+}(H_2O)_6 \cdots \text{ligand}] - E[M^{2+}(H_2O)_6] - E[\text{ligand}] + CP(BSSE)$$
(3)

where $E[\mathrm{M}^{2+}(\mathrm{H}_2\mathrm{O})_6\cdots\mathrm{ligand}]$, $E[\mathrm{M}^{2+}(\mathrm{H}_2\mathrm{O})_6]$, and $E[\mathrm{ligand}]$ are the electronic energies of the complex, hydrated metal ion, and ligand (carboxylate, phosphate, or guanine), respectively. CP(BSSE) is the counterpoise (CP) correction⁵⁶ for basis set superposition error (BSSE) calculated for the complex in vacuum. The binding energy for direct binding (BE_{direct}) explicitly accounts for the loss of a single water molecule and was calculated as:

$$BE_{\text{direct}} = E[M^{2+}(H_2O)_5 \cdots \text{ligand}] + E[H_2O] - E[M^{2+}(H_2O)_6]$$
$$- E[\text{ligand}]$$
$$+ CP(BSSE)$$

where $E[{\rm H_2O}]$ was the electronic energy of a water molecule. The energetic penalty of removing a first-solvation shell water molecule from the divalent metal ion is explicitly taken into account when calculating DFT binding energies, which reduces the binding energy for direct binding compared to indirect binding. The deformation energy is the energy required to distort the structure of each component prior to forming the complex. Because optimized

geometries are used to calculate BEindirect and BEdirect, the deformation energy is included in the calculated binding energies. All DFT calculations were performed using Gaussian 09 electronic structure software⁵⁹ with the B3LYP functional⁶⁰⁻⁶² and the 6-311+G(d,p) basis set. Empirical dispersion was modeled by the GD3BJ function.⁶³ A combined explicit and continuum solvent model was used,64 where water molecules within the first solvation shell of each ion were modeled explicitly at the B3LYP/6-311+G(d,p) level of theory and bulk water was modeled as a dielectric continuum (arepsilon =78.355300 and $\varepsilon_{\infty}=1.777849$) using the SMD continuum model⁶⁵ and the van der Waals (VDW) solute cavity⁶⁴ with unscaled SMD atomic radii.65 Geometries of hydrated metal ions Mg2+(H2O)6, $Ni^{2+}(H_2O)_6$, and $Co^{2+}(H_2O)_6$ and complexes of these ions indirectly and directly bound to carboxylate (CH₃COO⁻), phosphate ((CH₃)₂PO₄⁻), and guanine (2-amino-9H-purin-6(1H)-one) were optimized and validated as local minima on their respective electronic potential energy surfaces using harmonic frequency analysis. The Mg²⁺, Ni²⁺, and Co²⁺ species were modeled in their ground electronic spin states: singlet, triplet, and quartet, respectively. The stability of the DFT wavefunction was validated for Ni²⁺ and Co²⁺ species. The Cartesian coordinates of optimized geometries are provided in the ESI. Optimized geometries of the hydrated metal ions reproduce experimental metal ion-water oxygen distances (Table S1). Although DFT methods may overestimate the binding energy of divalent metal ions,57, 66, 67 the qualitative trends among different metal-ligand complexes can provide physical insight into the overall mechanism of metal ion-mediated DNA adsorption. Here, the DFT binding energies of Mg²⁺ species are similar in magnitude as the experimental binding free energy of Mg2+ bound to single-strand DNA (Table S2).68 Omitting empirical dispersion improves this agreement between calculated and experimental values, but does not alter the trends in the relative binding energies of Mg²⁺ species (Table S2).

The minimum-energy DFT structures used here to calculate binding energies have some limitations. Because the geometric structures are optimized at 0 K and no thermal effects are considered, the calculated binding energies do not account for temperature and entropy effects. The small molecules used to model the binding sites on DNA and the SAM neglect some interactions, such as extended hydration, nucleobase pairing and stacking, and the binding of more than one carboxylate group per divalent cation. Simultaneous binding of the divalent metal ion to other species, such as Tris or acetate, is also neglected (i.e., only free divalent metal ions are considered). Despite these limitations, the small-molecule DFT binding energies reported here are expected to represent the local metal-ligand interactions that govern the adsorption of free divalent metal ions to specific binding sites along DNA and the MUDA surface. This assumption is based on previous work that demonstrates that minimum-energy complexes of small-molecules accurately reproduce key physical properties of interfacial metal ion adsorption.44

Results and discussion

A long double-stranded DNA was tethered to the AFM tip using DNA templated crosslinking (Figures S1 and S2).^{29, 69} In the presence of divalent cations, such as Ni²⁺, constant-force plateaus were observed

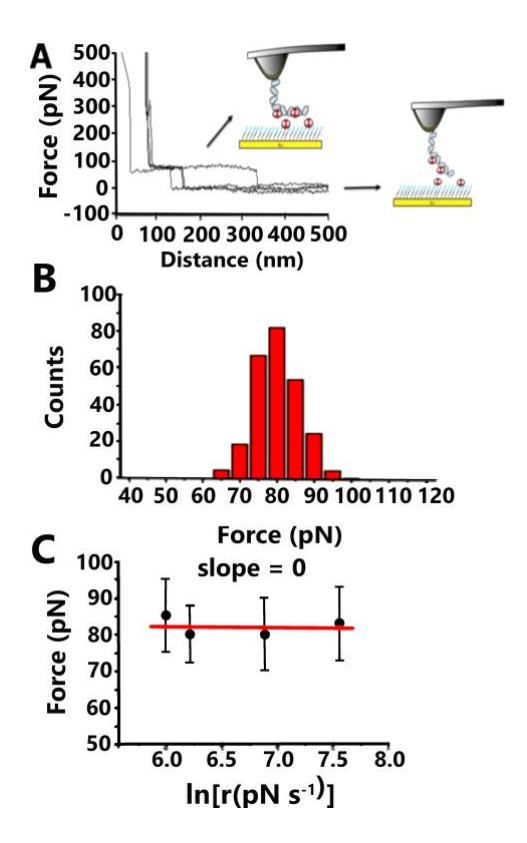


Figure 1. Single-molecule force spectra between DNA and MUDA SAM under an aqueous Ni²+ imaging buffer (NB, 5mM Ni(II) acetate, 4 mM Tris(hydroxymethyl)aminomethane acetate (TrisAc), 0.1 mM EDTA, pH 8.0). Typical force-extension curves for (A) single plateau force. (B) Distribution of the plateau force. The average force is estimated as 80 \pm 10 pN (n = 300). (C) Loading rate dependence of plateau force.

as the tip repeatedly approached and retracted from the surface (Figure 1A). In contrast, tips that were not functionalized with DNA did not display such plateaus (Figure S3). Moreover, DNA tethered tips in a 2 M NaAc buffer did not display any plateau force (Figure S4).

To quantify the strength of DNA-surface interactions, in the presence of the divalent cations, a series of force spectra (several hundred force-distance curves for each condition) were acquired and statistically analyzed. The measured plateau force is 80 \pm 10 pN under the Ni2+ imaging buffer (NB, 5 mM Ni(II) acetate, 4 mM Tris(hydroxymethyl)aminomethane acetate (TrisAc), 0.1 mM EDTA) (Figure 1B). These plateau forces are independent of the loading rate (Figure 1C). In SMFS, the potential energy landscape of nonequilibrium bond dissociation can be probed by varying the loading rate, which affects the probability of crossing over the free energy barrier.70 For non-equilibrium bond breaking, the most probable rupture force shifts to a higher value as the loading rate increases. Therefore, the observed independence on the loading rate suggests that the molecules are being peeled off the surface in a quasi-equilibrium manner, i.e., the time scale for the adsorbed segments to rearrange on the surface is much shorter than the time scale of desorption. $^{28,\;71,\;72}$ Therefore , the plateau forces reported here reflect the strength of dsDNA adsorption in the presence of divalent cations in a quasi-equilibrium state. It is known that dsDNAs undergo a transition to an overstretched state when the stretching force exceeds 65 pN. ^{73, 74} In the presence of Ni²⁺, the desorption force

may exceed the threshold under certain conditions. However, the overstretching is not expected to significantly alter the desorption force. As overstretching can only take place after the base-pair leaves the surface, the desorption force is not appreciably affected by overstretching. Previous experimental and theoretical studies of single molecule force spectroscopy established that a constant force plateau means the molecule is being peeled off the surface with negligible friction. 28, 71, 72, 75-80 As the dsDNA molecule is being peeled off the surface and only a single segment (likely one or a few basepairs) is under significant tension (Figure S5), the desorption force is determined by the force required to dissociate the last unit segment off the surface. 72, 78, 79 Our assumption that the overstretching of the DNA segment does not significantly affect the desorption force is supported by observation of desorption forces well above 65 pN (Figure 1B). Also, there is a lack of abrupt changes in the desorption force vs ionic strength curve and the desorption force vs cation concentration curve near 65 pN (Figure S6).

The equilibrium nature of the desorption process allows us to calculate E_b , the binding free energy from the desorption force (f) using (5), where L is the length of each base pair (0.332 nm/bp for DNA):

$$E_b = fL/k_B T \tag{5}$$

The average binding energy under 5 mM Ni²⁺, 6.33 \pm 0.79 k_BT /bp, corresponds to 3.16 \pm 0.40 k_BT /charge, since each base pair contains two phosphate groups. This value is below 7-9 k_BT /charge, the maximum attraction between two anionic surfaces when the adsorbed multivalent cations are in a perfectly staggered configuration.²¹

An important point to consider is the protonation state of MUDA. The large binding energy in the Ni²⁺ buffer suggests that the MUDA surface is deprotonated, allowing the divalent cations to bind to the surface. The measured pH of the Ni²⁺ buffer is 8.0. The pKa of carboxyl groups in a homogeneous solution is about 5, which ensures complete ionization under the measured pH. Although the pKa of carboxyl groups in a monovalent buffer increases to 6-7 due to electrostatic interactions that increase the local concentration of H⁺,⁸¹ divalent cations are known to promote the deprotonation of carboxyl groups in long chain fatty acids at interfaces because the binding of divalent cations can increase the surface potential, which depletes the number of hydronium ions near the surface and favors

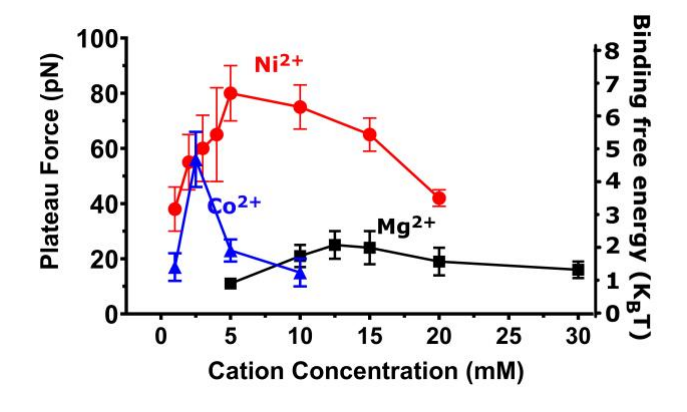


Figure 2. Concentration dependence of the plateau force and binding free energy for three divalent cations, Mg^{2+} , Ni^{2+} and Co^{2+} . The concentration of TrisAc was held constant at 4 mM.

the deprotonated state. Indeed, the pKa of COOH in a monolayer under a buffer containing mM concentrations of Ca²⁺ cations was found to be about 5, which is similar to solution phase values.⁸¹ Numerous vibrational spectroscopy studies show that fatty acid monolayers at solid-liquid and air-liquid interfaces are completely deprotonated in mM Ca²⁺ solutions.⁸²⁻⁸⁴ The binding constant of Mg²⁺ to carboxylate groups is found to be nearly identical to that of Ca²⁺.⁸⁵, ⁸⁶ Hence, we assume that most of the COOH groups are deprotonated in Mg²⁺ as well. Transition metal cations such as Co²⁺ and Ni²⁺ have stronger binding to carboxyl groups and hence should more readily deprotonate carboxyl groups. Indeed, spectroscopic studies show that carboxyl terminated monolayers are completely deprotonated in Co²⁺ ⁸⁴, ⁸⁷ and Ni²⁺.⁵⁵

It is important to understand how the binding energy of DNA to the surface depends on the identity of the cation as well as concentration. Quantitative measurement of how the DNA-surface interactions depend on the buffer composition will allow precise control of the DNA-surface interactions for practical applications. Moreover, the quantitative information will provide insights into the origin of the divalent-cation-induced attraction. We measured the binding energies of DNA mediated by three different metal cations, Ni²⁺, Mg²⁺, and Co²⁺ over a range of concentrations and different ionic strengths (Figure 2). The plateau forces/binding energies of all three metal ions increases, reaches a maximum near 1-10 mM, and then declines as the cation concentration increases. The decrease in binding energy is likely not caused by the increased ionic strength due to the addition of Ni²⁺ because a very similar overall dependence of adhesion force over Ni²⁺ concentration was observed at a constant ionic strength of 60 mM (Figure 3).

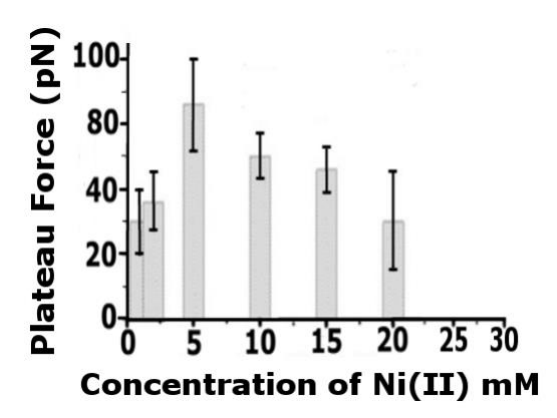


Figure 3. Plateau force as a function of the concentration of Ni $^{2+}$ under a fixed ionic strength of 60 mM. Plateau force histograms at 1 mM Ni(II) and 57 mM TrisAc, 2 mM Ni(II) and 54 mM TrisAc, 5 mM Ni(II) and 45 mM TrisAc, 10 mM Ni(II) and 30 mM TrisAc, 15 mM Ni(II) and 15 mM TrisAc, 20 mM Ni(II) and 0 mM TrisAc from left to right respectively. The concentration of TrisAc was adjusted to maintain the same ionic strength.

The DNA-surface binding energy for transition metal ions, Ni²⁺ and Co²⁺, peaks at a lower concentration than for the alkaline earth metal ion Mg²⁺ (Figure 2). Such concentration dependence can be readily explained by the counterion correlation mechanism. In this mechanism, the strongest counterion correlated attraction occurs when half of the adsorption sites are occupied by the cations, ^{19, 21, 24} *i.e.*, when the cation concentration is near its binding constant (K_D). As the density of adsorbed cation increases further, the correlated attraction is weakened. Transition metal cations are known have

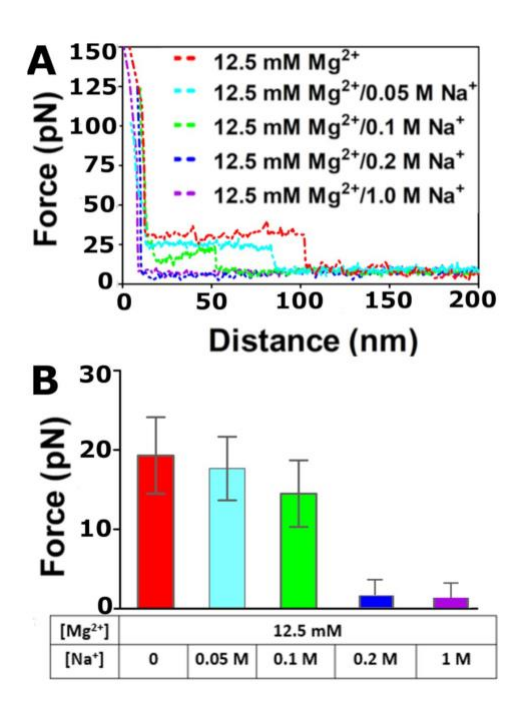


Figure 4. Effects of the buffer composition on the plateau force of dsDNA on MUDA SAM. (A) Plateau force as a function of the ionic strength. The concentration of Mg²⁺ was held constant at 12.5 mM. The ionic strength was varied by adjusting the concentration of NaAc. (B) Plateau force as a function of the concentration of Mg²⁺ and Na⁺. The concentration of TrisAc buffer was held constant at 12.5 mM.

lower K_D values for phosphate and carboxylate groups than Mg²⁺,^{88,} ⁸⁹ which is consistent with the binding energies for Ni²⁺ and Co²⁺ peaking at lower concentrations (2.5-5 mM) than for Mg²⁺ (12.5 mM). To further probe the nature of interactions, we added different amounts of monovalent salt NaAc to 12.5 mM Mg²⁺ and measured the corresponding plateau forces. The results showed that as the ionic strength increases, the DNA binding strength is diminished (Figure 4A). The force plateau was no longer observable with 0.2 M NaAc (Figure 4B). The decline of the plateau force with increasing ionic strength further supports the electrostatic origin of the divalent cation mediated attraction of DNA to the MUDA surface. A similar trend was observed when TrisAc was added to increase the ionic strength of 5 mM Ni2+ solution (Figure S4A). The observed dependence of binding energy on the ionic strength also suggests that the binding strength is not modulated by the protonation state of the SAM. A lower ionic strength should favor the protonated state of surface carboxyl groups⁷⁸ and hence should weaken the binding of DNA. E.g., the use of surface functionalities with a lower pKa could clarify the role of protonation in modulating the DNA binding. That the opposite trend is observed provides support for electrostatic attraction involving an ionized SAM surface.

It has been proposed that monovalent cations may alter DNA adhesion by competing with divalent cations for binding to DNA or the cationic surface.²⁰ Moreover, the deprotonated form of Tris may complex with the divalent cations. To investigate the role of monovalent ions in this process, both the ionic strength and the [Ni²⁺] were held constant, while the molar ratio of the monovalent salts (NaAc and TrisAc) was varied by nearly three orders of magnitude (Figure 5). The desorption force is nearly unchanged over the entire

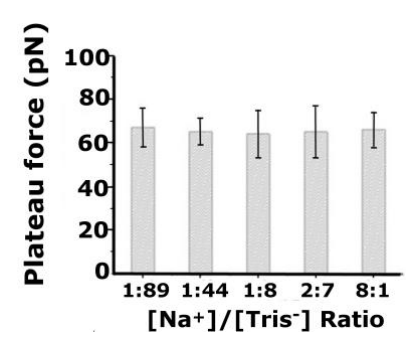


Figure 5. Plateau force as a function of the molar ratio of sodium acetate and TrisAc. The ionic strength was held constant at 60 mM and the concentration of Ni^{2+} was held constant at 5 mM.

range of the molar ratios studied even though Tris and Na $^+$ have substantially different ionic radii, $^{\sim}4$ Å and 2.2 Å. That the desorption force is independent of the type of monovalent cation suggests that monovalent cations do not directly participate in the DNA adsorption mechanism, but instead modulate counterion-correlation through electrostatic screening. Moreover, the results suggest that the deprotonated Tris does not complex with Ni $^{2+}$ to a significant degree under the conditions investigated.

Although the results support a counter ion correlation mechanism for the observed DNA adhesion, alternative mechanisms including image charge interactions (ICIs) and hydrogen bonding need to be considered. The charged DNA can polarize the gold substrate, creating image charges within the metal that attract DNA toward the surface. 90, 91 However, Gaub and coworkers observed negligible adhesion of dsDNA to a neutral OH terminated SAM on gold at the potential of zero charge, where ICIs should be similar to that between dsDNA and our carboxyl terminated SAMs.²⁸ Therefore, our observed DNA adhesion can not be explained by ICIs but is attributed to the carboxylate groups. Another possible DNA-surface interaction is hydrogen bonding between the phosphate groups of the dsDNA and the protonated carboxyl groups on the surface. To test this hypothesis, SMFS was performed with 1 M NaAc and 2 M NaAc (Figure S4). As the high ionic strength monovalent cation buffer can effectively screen electrostatic repulsion between the MUSA SAM and phosphate groups, a plateau force should be observable if there were substantial hydrogen bonding mediated attraction between the phosphate groups and protonated MUDA SAMs. Therefore, the lack of observable adhesion forces in a high ionic strength monovalent cation buffer rules out hydrogen bonding as a major contributor to the adhesion force between DNA and the MUDA surface (Figure S4). If hydrogen bonding between DNA and MUDA is not important in a monovalent cation buffer, it is even less likely to play a role in the presence of divalent cations, which disfavor such hydrogen bonding interactions by deprotonating the carboxyl groups. Additional discussion can be found in ESI.

Despite substantial evidence of an electrostatic origin of the attraction, the ion-specific effects shown in Figure 2 are difficult to explain by the existing electrostatics-based counterion correlation models, which predict similar binding energies for different divalent cations. $^{19,\ 21}$ Figure 2 demonstrates that the maximum adhesion force between DNA and MUDA decreases in the following order: Ni²+ > Co²+ > Mg²+. Here, we aim to

rationalize these ion-specific results using minimum-energy structures of relevant metal-ligand complexes. For example, at 5 mM, the DNA-surface binding energy in Ni²⁺ is 5 times as strong as that in Mg²⁺. Binding energies of three hydrated ions, Mg²⁺, Ni²⁺, and Co²⁺, bound to a carboxylate anion, phosphate anion, and guanine nucleobase were computed using DFT (Figure 6). Previous small-molecule DFT studies have previously focused on Mg²⁺ ions binding to DNA binding sites (i.e., phosphate and guanine),52,57,58,66,67,92-94 and a few studies included Ni²⁺ or Co²⁺ ions.^{52, 67, 93} DFT studies that investigate carboxylate binding to divalent metal ions are limited. 58, 84, 85, 95 Here, for the first time, consistent computational methods are used to model Mg²⁺, Ni²⁺, and Co²⁺ binding to a carboxylate anion, phosphate anion, and guanine nucleobase, which allows direct comparison of the relative binding energies of each metal-ligand complex potentially involved in DNA adsorption onto carboxylate terminated SAMs.

The ion-bridging mechanism implies that differences in local metal-ligand binding energy will influence the overall strength of DNA adsorption. Given that only the phosphate DNA binding sites are physically accessible to form ion-bridging complexes with the carboxylate surface, the metal-phosphate and metal-carboxylate binding energies must vary for different metal ions for ion-bridging to contribute to the overall mechanism. Metal ions may interact with a binding site through indirect binding (i.e., outer-sphere or solvent-shared ion pair) or direct binding i.e., inner-sphere or contact ion pair). Indirect binding consists of hydrogen bonds between water molecules in the first solvation shell of the metal ion and the binding site. Direct binding occurs when the binding site displaces at least one water molecule from the first solvation shell of the metal ion to form a direct contact with the metal ion. For a given binding

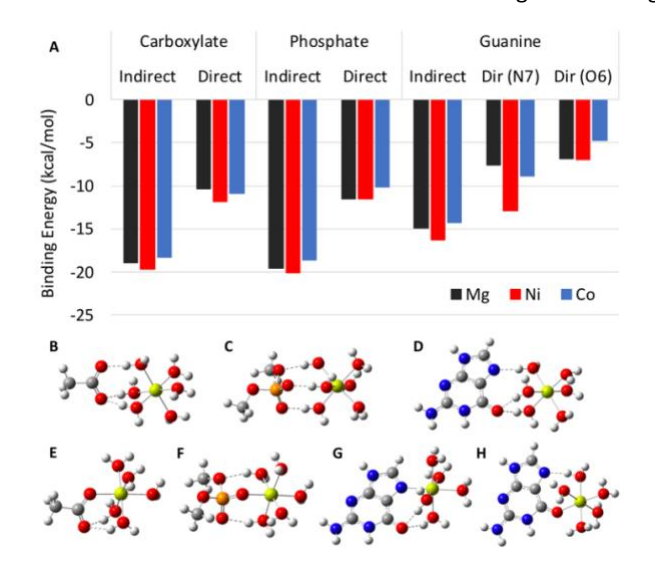
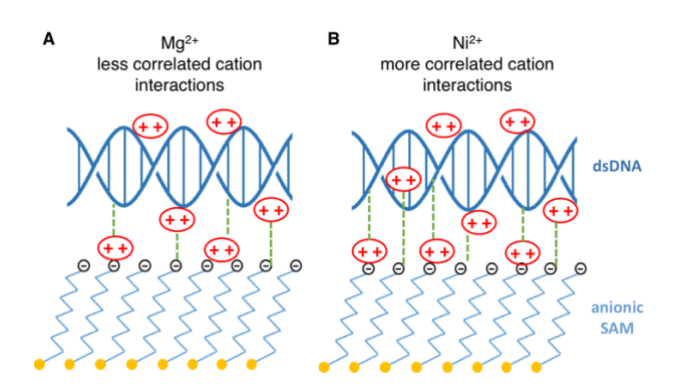


Figure 6. (A) Calculated binding energies (kcal/mol) of $[Mg(H_2O)_6]^{2+}$, or $[Co(H_2O)_6]^{2+}$ indirectly and directly bound to carboxylate, phosphate, or guanine at the B3LYP/6-311+g(d,p) level of theory with GD3B empirical dispersion. Optimized geometries of the binary Mg^{2+} complexes at the same level of theory are shown in panels B-H, including indirect binding of $[Mg(H_2O)_6]^{2+}$ to (B) carboxylate, (C) phosphate, or (D) guanine and monodentate direct binding of $[Mg(H_2O)_5]^{2+}$ to (E) carboxylate, (F) phosphate, (G) the guanine N7 atom or (H) the guanine O6 atom. Mg, P, O, N, C, and H atoms are shown as yellow, orange, red, blue, grey, and white spheres, respectively.

motif (i.e., direct or indirect), our calculated carboxylate and phosphate binding energies are similar in magnitude for a given ion (Figure 6). In addition, the binding energy differences between metal ions for a given metal-carboxylate or metalphosphate complex are small (< 2 kcal/mol). Ternary complexes that explicitly model two ligands binding to a divalent metal ion revealed similar results (Figure S7). These small differences in binding energies suggest that local ion-bridging structures do not significantly contribute to the measured differences in the plateau forces and the overall mechanism of DNA adsorption. However, the DFT results do support an ion-correlation mechanism that is modulated by the divalent metal ion affinity for different DNA binding sites. The guanine nucleobase has a stronger preference for Ni²⁺ compared to the other divalent metal ions (Figure 6), especially for direct binding to the N7 atom of guanine (~5 kcal/mol). This result is in agreement with previous experimental⁴⁸ and DFT studies.^{52, 93} Computed atomic charges reveal that Ni²⁺ exhibits more significant charge transfer than Co²⁺ or Mg²⁺, which correlates with the increased binding energy (Figure S8). The fact that Ni²⁺ has an energetic preference for the N7 atom of guanine is consistent with K_D values of Ni²⁺ binding to a phosphate moiety with and without a nucleobase.89 Previous Raman spectroscopy studies of metal cation binding to DNA have also shown that transition metal cations can bind to the N7 site of purines. 48, 96 This affinity for the N7 atom may provide an additional binding site for divalent metal ions along DNA that is more favorable for Ni²⁺ compared to Co²⁺ or Mg²⁺. In sum, the DFT calculations provide insight into the relative binding strengths shown in Figure 2, rationalizing that the Ni²⁺ binding energy is larger due the presence of additional binding site for Ni2+ on guanine. The calculations also support the correlated binding mechanism proposed in Scheme 2 by showing that the strength of the binding for all three divalent cations is similar for the carboxylate and the phosphate ligands, but that the potential for direct DNA binding for Ni²⁺ leads to additional correlated binding sites.

Overall, our DFT study of metal-ligand interactions and quantitative measurement of DNA binding energies support an electrostatic counterion correlation mechanism that is influenced by the divalent metal ion's affinity for DNA binding sites. First, the independence of the desorption force over the loading rate (Figure 1C) is not consistent with the direct ion bridging mechanism. The desorption force of DNA that is bridged by metal cations to the surface would be loading-rate dependent, as the desorption would require the breaking of the metal-ligand bonds, which is an activated process.⁹⁷ Similar loading-rate-independent plateau forces were previously observed for polyelectrolytes that adhere to the surface due to electrostatic interactions.^{28, 72} Second, the significant decrease in DNA binding energy with increasing ionic strength (Figure 4) also supports an electrostatic origin to this process (Scheme 1A). If metal ion bridging (Scheme 1B) were responsible for DNA binding to the surface, the DNA binding energy should increase with increasing ionic strength as the metal-ligand interactions are only moderately affected by the ionic strength, 98 whereas an increase in ionic strength would screen the electrostatic repulsion between the DNA and the anionic SAM and increase the overall attraction. Third, DFT calculations reveal small differences in the binding energies of



Scheme 2. Proposed counterion correlation mechanism for cation-mediated DNA adsorption that is consistent with the observed ion-specific effects. (A) Mg^{2+} may induce less correlated cation interactions than (B) Ni^{2+} between dsDNA and anionic SAM. Divalent cations are shown as red ovals. Correlated cation interactions are represented by dashed green lines.

various metal cations to the same ligands (Figure 6), which alone do not account for the substantially different DNA binding energies observed for the three cations (Figure 2). Fourth, the divalent cation concentration dependence of the DNA binding energy provides support for the counterion correlation mechanism. In this mechanism, the strongest counterion correlated attraction occurs when half of the adsorption sites are occupied by the cations, 19, 21, 24 *i.e.*, when the cation concentration is near its K_D . For all three cations, the DNA binding energy peaks within the 1-10 mM divalent cation concentration range (Figure 2), which is consistent with the K_D values for divalent cations binding to phosphate⁶⁵ and carboxylate groups.⁷⁰ Fifth, the divalent cation concentrations for peak DNA binding with Ni²⁺ and Co²⁺ are lower than that with Mg²⁺ (Figure 2). This trend is consistent with the observation that transition metal cations have lower K_D values for phosphate and carboxylate groups than Mg²⁺.^{88,} ⁸⁹ The trend is also consistent with the observations that the zeta potential increases as more divalent cations are added and a rapid increase occurs at concentrations of a few mM in Ni2+. In contrast, the increase in zeta potential is more gradual and zeta potentials at the same concentrations are lower in Mg²⁺ (Figure S9). Hence, counterion correlation dominates this process and ion-specific binding preferences influence the electrostatic attraction.

An important question is why Ni²⁺ produces a substantially higher peak DNA binding energy than Mg2+ (Figure 2). Counterion correlation mediated attraction between two anionic surfaces is predicted to produce a maximum binding energy of 7- $8 k_B T / \text{charge},^{19, 21}$ regardless of the cation type. However, the existing model assumes that the binding sites are uniform across the two surfaces. Due to the mismatch between helical arrangement of phosphate groups and the densely packed carboxylate groups on MUDA SAMs, it is not possible for cations between DNA and the MUDA SAM to assume a perfectly staggered configuration to achieve the theoretical maximum binding energy. Indeed, the alkaline earth metal ion Mg²⁺, which does not have a significant preference for the N7 atom of guanine and binds primarily to the phosphate groups (Scheme 2A), produces DNA binding free energy up to 1 k_BT /charge. In contrast, DFT calculations show that in addition to binding to phosphate, Ni2+ preferentially binds to the N7 atom of guanine, providing an additional binding site for Ni2+ along DNA, which may induce more correlated ion interactions, thus, stronger attraction

(Scheme 2B). With this evidence, taken all together, we propose that metal-ion mediated DNA adsorption to a charged surface is facilitated by a counterion correlation mechanism that is dependent on the strength and energetically preferred binding site of metalligand interactions.

Conclusions

In summary, by combining quantitative measurement of binding energies and DFT calculations of metal-ligand interactions, our study clarifies a number of questions concerning interactions that are responsible for multivalent-cation-mediated attraction between an anionic polyelectrolyte and an anionic surface. Our results also explain why the interaction strengths are ion-specific. The study underscores the need to account for the atomic scale structure of polyelectrolyte molecules and surfaces to accurately predict the attractive interactions. Surface specific spectroscopic techniques,^{38,} 83 including X-ray reflectometry and spectrometry, 99 may be used to directly probe the binding of cations to anionic surfaces in proximity. Our approach can be extended to a wide range of metal ions, surfaces with tailored functional groups, and polyelectrolytes with different chemical functionalities and structural motifs, which would uncover additional mechanistic details of the multivalent cation mediated attraction. While most studies of biomolecular selfassembly have relied on self-assembly in a homogeneous solution, 100-102 self-assembly at surfaces is appealing for numerous reasons, including compatibility with in situ imaging, ease of purification, and the potential to integrate with top down approaches for device applications. 10 New insights derived from our model can guide precise tailoring of biomolecule-surface interactions in the self-assembly of complex structures at the solid-liquid interface^{5, 7, 10} and are potentially relevant to a broad spectrum of cation-mediated attractions between macromolecules or their assemblies.12,14

Electronic Supplementary Information (ESI) available.

Experimental materials and methods, schematic illustration of the generation of the DNA target, modification of AFM tip with long dsDNA, force-distance curve of an AFM tip that is not functionalized with dsDNA, effect of buffer and SAM composition on force measurements, validation of computational methods, structural analysis of binary metalligand complexes, binding energies and example structures of ternary metal-ligand complexes (PDF), Cartesian coordinates of optimized structures (ZIP)

Conflicts of interest

There are no conflicts to declare.

Acknowledgements

T.Y., X.H., and Q.G. acknowledge support by the National Science Foundation (CHE-1808213) for measurement of single molecule force spectroscopy and the Department of Energy (DE-SC0020961) for data analysis. J.R.V. acknowledges support by NSF-CREST: Center for Cellular and Biomolecular Machines at the University of

California, Merced (NSF-HRD-2112675). C.I. acknowledges support by the National Science Foundation (Grant No. CHE-1955656).

References

- M. Hayashi and K. M. Yamada, J Biol Chem, 1982, 257, 5263-5267.
- 2. O. Matsarskaia, F. Roosen-Runge and F. Schreiber, *Chemphyschem*, 2020, **21**, 1742-1767.
- 3. H. G. Hansma and D. E. Laney, *Biophys J*, 1996, **70**, 1933-1939.
- 4. X. P. Sun, S. H. Ko, C. A. Zhang, A. E. Ribbe and C. D. Mao, *J Am Chem Soc*, 2009, **131**, 13248-13249.
- 5. S. Woo and P. W. K. Rothemund, *Nat Commun*, 2014, **5**, 5610.
- 6. Y. Suzuki, M. Endo and H. Sugiyama, *Nat Commun*, 2015, **6**, 8052.
- 7. H. Pyles, S. Zhang, J. J. De Yoreo and D. Baker, *Nature*, 2019, **571**, 251.
- 8. G. R. Abel, E. A. Josephs, N. Luong and T. Ye, *J Am Chem Soc*, 2013, **135**, 6399-6402.
- 9. Q. F. Gu, W. Nanney, H. H. Cao, H. Y. Wang and T. Ye, *J Am Chem Soc*, 2018, **140**, 14134-14143.
- H. H. Cao, G. R. Abel, Q. F. Gu, G. A. V. Gueorguieva, Y. H. Zhang, W. A. Nanney, E. T. Provencio and T. Ye, *ACS Nano*, 2020, 14, 5203-5212.
- S. Patel, N. Ashwanikumar, E. Robinson, Y. Xia, C. Mihai,
 J. P. Griffith, S. G. Hou, A. A. Esposito, T. Ketova, K.
 Welsher, J. L. Joyal, O. Almarsson and G. Sahay, *Nat Commun*, 2020, 11, 3435.
- 12. R. C. Weisenberg, Science, 1972, 177, 1104-1105.
- 13. R. W. Wilson and V. A. Bloomfield, *Biochemistry*, 1979, **18**, 2192-2196.
- I. Hamilton, M. Gebala, D. Herschlag and R. Russell, J Am Chem Soc, 2022, 144, 1718-1728.
- B. Dai, S. G. Kang, T. Huynh, H. Z. Lei, M. Castelli, J. Hu, Y. Zhang and R. H. Zhou, *P Natl Acad Sci USA*, 2013, **110**, 8543-8548.
- 16. C. Ha, J. Ryu and C. B. Park, *Biochemistry*, 2007, **46**, 6118-6125.
- A. Ortiz, J. A. Killian, A. J. Verkleij and J. Wilschut, *Biophys J*, 1999, 77, 2003-2014.
- J. N. Israelachvili, Intermolecular and surface forces, Academic Press, Burlington, MA, 3rd edn., 2011.
- 19. J. J. Arenzon, J. F. Stilck and Y. Levin, *Eur Phys J B*, 1999, **12**, 79-82.
- D. Pastre, O. Pietrement, P. Fusil, F. Landousy, J. Jeusset,
 M. O. David, C. Hamon, E. Le Cam and A. Zozime, *Biophys J*, 2003, 85, 2507-2518.
- 21. I. Rouzina and V. A. Bloomfield, *J Phys Chem-Us*, 1996, **100**, 9977-9989.
- 22. G. S. Manning, *Quarterly reviews of biophysics*, 1978, **11**, 179-246.
- 23. R. J. Mashl and N. Gronbech-Jensen, *J Chem Phys*, 1998, **109**, 4617-4623.
- 24. B. Hribar and V. Vlachy, *J Phys Chem B*, 2000, **104**, 4218-4221.
- 25. N. H. Thomson, S. Kasas, B. Smith, H. G. Hansma and P. K. Hansma, *Langmuir*, 1996, **12**, 5905-5908.
- S. Kempter, A. Khmelinskaia, M. T. Strauss, P. Schwille, R. Jungmann, T. Liedl and W. Bae, ACS Nano, 2019, 13, 996-1002.
- 27. A. Noy, Curr Opin Chem Biol, 2011, **15**, 710-718.

- 28. M. Erdmann, R. David, A. Fornof and H. E. Gaub, *Nat Nanotechnol*, 2010, **5**, 154-159.
- 29. G. R. Abel, B. H. Cao, J. E. Hein and T. Ye, *Chem Commun*, 2014, **50**, 8131-8133.
- 30. E. A. Josephs and T. Ye, *Nano Lett*, 2012, **12**, 5255-5261.
- 31. E. A. Josephs and T. Ye, *ACS Nano*, 2013, **7**, 3653-3660.
- 32. R. Levy and M. Maaloum, *Nanotechnology*, 2002, **13**, 33-37.
- 33. C. Rivetti, M. Guthold and C. Bustamante, *J Mol Biol*, 1996, **264**, 919-932.
- 34. P. A. Wiggins, T. Van der Heijden, F. Moreno-Herrero, A. Spakowitz, R. Phillips, J. Widom, C. Dekker and P. C. Nelson, *Nat Nanotechnol*, 2006, **1**, 137-141.
- 35. C. Leung, A. Bestembayeva, R. Thorogate, J. Stinson, A. Pyne, C. Marcovich, J. L. Yang, U. Drechsler, M. Despont, T. Jankowski, M. Tschope and B. W. Hoogenboom, *Nano Lett*, 2012, **12**, 3846-3850.
- 36. S. Ido, K. Kimura, N. Oyabu, K. Kobayashi, M. Tsukada, K. Matsushige and H. Yamada, *ACS Nano*, 2013, **7**, 1817-1822
- 37. S. Sam, S. Krem, J. Lee and D. Kim, *J Phys Chem B*, 2022, **126**, 643-649.
- M. G. V. de Vasquez, B. A. W. Rudd, M. D. Baer, E. E. Beasley and H. C. Allen, *J Phys Chem B*, 2021, 125, 11308-11319.
- 39. T. Rios-Carvajal, N. Bovet, K. Bechgaard, S. L. S. Stipp and T. Hassenkam, *Langmuir*, 2019, **35**, 16153-16163.
- 40. W. Y. Wang, J. L. Zhu, Q. Huang, L. Zhu, D. Wang, W. M. Li and W. J. Yu, *Molecules*, 2024, **29**, 308.
- L. M. da Costa, S. R. Stoyanov, R. N. Damasceno and J. W.
 D. Carneiro, *Int J Quantum Chem*, 2013, 113, 2621-2628.
- 42. M. V. M. Meuser, D. G. S. Quattrociocchi, L. M. Da Costa, G. B. Ferreira and J. W. D. Carneiro, *Polyhedron*, 2015, **102**, 193-200.
- D. S. G. Quattrociocchi, J. W. D. Carneiro, G. B. Ferreira, S.
 R. Stoyanov, R. N. Damasceno and L. M. da Costa, Chemistryselect, 2017, 2, 4617-4625.
- J. K. Denton, P. J. Kelleher, M. A. Johnson, M. D. Baer, S. M. Kathmann, C. J. Mundy, B. A. W. Rudd, H. C. Allen, T. H. Choi and K. D. Jordan, P Natl Acad Sci USA, 2019, 116, 14874-14880.
- 45. T. Dudev and C. Lim, *J Am Chem Soc*, 2006, **128**, 1553-1561.
- 46. V. Sladek and I. Tvaroska, *J Phys Chem B*, 2017, **121**, 6148-6162.
- 47. M. Langlais, H. A. Tajmirriahi and R. Savoie, *Biopolymers*, 1990, **30**, 743-752.
- 48. J. Duguid, V. A. Bloomfield, J. Benevides and G. J. Thomas, *Biophys J*, 1993, **65**, 1916-1928.
- 49. V. A. Buckin, B. I. Kankiya, D. Rentzeperis and L. A. Marky, *J Am Chem Soc*, 1994, **116**, 9423-9429.
- 50. J. A. Subirana and M. Soler-Lopez, *Annu Rev Bioph Biom*, 2003, **32**, 27-45.
- 51. R. Ahmad, H. Arakawa and H. A. Tajmir-Riahi, *Biophys J*, 2003, **84**, 2460-2466.
- 52. V. Andrushchenko and P. Bour, *J Phys Chem B*, 2009, **113**, 283-291.
- 53. F. Leonarski, L. D'Ascenzo and P. Auffinger, *Inorg Chim Acta*, 2016, **452**, 82-89.
- 54. M. P. Long, S. Alland, M. E. Martin and C. M. Isborn, *Phys Chem Chem Phys*, 2020, **22**, 5584-5596.
- 55. J. Simon-Kutscher, A. Gericke and H. Huhnerfuss, *Langmuir*, 1996, **12**, 1027-1034.
- 56. S. F. Boys and F. Bernardi, *Mol Phys*, 2002, **100**, 65-73.

- 57. A. S. Petrov, J. Funseth-Smotzer and G. R. Pack, *Int J Quantum Chem*, 2005, **102**, 645-655.
- 58. K. Walden, M. E. Martin, L. LaBee and M. P. Long, *J Phys Chem B*, 2021, **125**, 12135-12146.
- M. Frisch, G. Trucks, H. Schlegel, G. Scuseria, M. Robb, J. Cheeseman, G. Scalmani, V. Barone, B. Mennucci and G. Petersson, *Gaussian Inc. Wallingford CT*, 2009, 106.
- 60. A. D. Becke, *J Chem Phys*, 1993, **98**, 5648-5652.
- 61. A. D. Becke, Phys Rev A, 1988, 38, 3098-3100.
- 62. C. T. Lee, W. T. Yang and R. G. Parr, *Phys Rev B*, 1988, **37**, 785-789.
- 63. S. Grimme, S. Ehrlich and L. Goerigk, *J Comput Chem*, 2011, **32**, 1456-1465.
- 64. J. Tomasi, B. Mennucci and R. Cammi, *Chemical Reviews*, 2005, **105**, 2999-3093.
- 65. A. V. Marenich, C. J. Cramer and D. G. Truhlar, *J Phys Chem B*, 2009, **113**, 6378-6396.
- 66. A. S. Petrov, G. R. Pack and G. Lamm, *J Phys Chem B*, 2004, **108**, 6072-6081.
- 67. R. Oliva and L. Cavallo, *J Phys Chem B*, 2009, **113**, 15670-15678.
- 68. J. G. Holland, D. S. Jordan and F. M. Geiger, *J Phys Chem B*, 2011, **115**, 8338-8345.
- 69. G. R. Abel, Z. A. Calabrese, J. Ayco, J. E. Hein and T. Ye, *Bioconjugate Chem*, 2016, **27**, 698-704.
- O. K. Dudko, G. Hummer and A. Szabo, P Natl Acad Sci USA, 2008, 105, 15755-15760.
- 71. S. Manohar, A. R. Mantz, K. E. Bancroft, C. Y. Hui, A. Jagota and D. V. Vezenov, *Nano Lett*, 2008, **8**, 4365-4372.
- 72. T. Hugel, M. Grosholz, H. Clausen-Schaumann, A. Pfau, H. Gaub and M. Seitz, *Macromolecules*, 2001, **34**, 1039-1047.
- 73. S. B. Smith, Y. J. Cui and C. Bustamante, *Science*, 1996, **271**, 795-799.
- 74. J. van Mameren, P. Gross, G. Farge, P. Hooijman, M. Modesti, M. Falkenberg, G. J. L. Wuite and E. J. G. Peterman, *P Natl Acad Sci USA*, 2009, **106**, 18231-18236.
- 75. M. Seitz, C. Friedsam, W. Jostl, T. Hugel and H. E. Gaub, *Chemphyschem*, 2003, **4**, 986-990.
- 76. L. Sonnenberg, Y. F. Luo, H. Schlaad, M. Seitz, H. Colfen and H. E. Gaub, *J Am Chem Soc*, 2007, **129**, 15364-15371.
- M. Geisler, B. N. Balzer and T. Hugel, Small, 2009, 5, 2864-2869.
- 78. S. Iliafar, D. Vezenov and A. Jagota, *Langmuir*, 2013, **29**, 1435-1445.
- 79. R. R. Netz and J. F. Joanny, *Macromolecules*, 1999, **32**, 9013-9025.
- 80. X. L. Kou, W. Zhang and W. K. Zhang, *ACS Appl Mater Inter*, 2016, **8**, 21055-21062.
- 81. R. Schweiss, D. Pleul, F. Simon, A. Janke, P. B. Welzel, B. Voit, W. Knoll and C. Werner, *J Phys Chem B*, 2004, **108**, 2910-2917.
- 82. A. Gericke and H. Huhnerfuss, *Thin Solid Films*, 1994, **245**, 74-82.
- 83. B. A. W. Rudd, A. S. Vidalis and H. C. Allen, *Phys Chem Chem Phys*, 2018, **20**, 16320-16332.
- 84. T. Bala, B. L. V. Prasad, M. Sastry, M. U. Kahaly and U. V. Waghmare, *J Phys Chem A*, 2007, **111**, 6183-6190.
- D. M. de Oliveira, S. R. Zukowski, V. Palivec, J. M. Henin,
 H. Martinez-Seara, D. Ben-Amotz, P. Jungwirth and E.
 Duboue-Dijon, Phys Chem Chem Phys, 2020, 22, 24014-24027.
- 86. J. W. Bunting and K. M. Thong, *Can J Chemistry*, 1970, **48**, 1654.

- 87. Y. C. Wang, X. Z. Du, L. Guo and H. J. Liu, *J Chem Phys*, 2006, **124**, 134706.
- 88. J. Kherb, S. C. Flores and P. S. Cremer, *J Phys Chem B*, 2012, **116**, 7389-7397.
- 89. H. Sigel and D. B. McCormick, *Accounts of Chemical Research*, 1970, **3**, 201-208.
- 90. H. Heinz, K. C. Jha, J. Luettmer-Strathmann, B. L. Farmer and R. R. Naik, *J R Soc Interface*, 2011, **8**, 220-232.
- 91. I. L. Geada, H. Ramezani-Dakhel, T. Jamil, M. Sulpizi and H. Heinz, *Nat Commun*, 2018, **9**, 716.
- 92. L. Rulisek and J. Sponer, *J Phys Chem B*, 2003, **107**, 1913-1923.
- 93. Y. Zhang and K. X. Huang, J Mol Struc-Theochem, 2007, **812**, 51-62.
- 94. I. Solt, I. Simon, A. G. Csaszar and M. Fuxreiter, *J Phys Chem B*, 2007, **111**, 6272-6279.
- 95. A. Y. Mehandzhiyski, E. Riccardi, T. S. van Erp, T. T. Trinh and B. A. Grimes, *J Phys Chem B*, 2015, **119**, 10710-10719.
- 96. J. G. Duguid, V. A. Bloomfield, J. M. Benevides and G. J. Thomas, *Biophys J*, 1995, **69**, 2623-2641.
- 97. X. Hao, N. Zhu, T. Gschneidtner, E. Ö. Jonsson, J. Zhang, K. Moth-Poulsen, H. Wang, K. S. Thygesen, K. W. Jacobsen and J. Ulstrup, *Nat Commun*, 2013, **4**, 1-10.
- 98. P. G. Daniele, C. Rigano and S. Sammartano, *Analytical Chemistry*, 1985, **57**, 2956-2960.
- 99. P. Fenter, C. Park, K. L. Nagy and N. C. Sturchio, *Thin Solid Films*, 2007, **515**, 5654-5659.
- 100. Y. G. Ke, L. L. Ong, W. M. Shih and P. Yin, *Science*, 2012, **338**, 1177-1183.
- 101. F. Hong, F. Zhang, Y. Liu and H. Yan, *Chemical Reviews*, 2017, **117**, 12584-12640.
- 102. N. C. Seeman, Annu Rev Biochem, 2010, **79**, 65-87.